

Energy Transfer in the Major Intrinsic Light-Harvesting Complex from *Amphidinium carterae*[†]

Tomáš Polívka,^{*,‡,§,||} Ivo H. M. van Stokkum,[‡] Donatas Zigmantas,^{#,∇} Rienk van Grondelle,[‡] Villy Sundström,^{||} and Roger G. Hiller[○]

Institute of Physical Biology, University of South Bohemia, Czech Republic, Institute of Plant Molecular Biology, Czech Academy of Sciences, Czech Republic, Department of Chemical Physics, Lund University, Sweden, Department of Physics and Astronomy, Vrije Universiteit, Amsterdam, The Netherlands, Department of Chemistry, University of California, Berkeley, California, Physical Biosciences Division, Lawrence Berkeley National Laboratory, Berkeley, California 94720, and Department of Biological Sciences, Macquarie University, NSW 2109, Australia

Received February 8, 2006; Revised Manuscript Received April 3, 2006

ABSTRACT: Carbonyl carotenoids are important constituents of the antenna complexes of marine organisms. These carotenoids possess an excited state with a charge-transfer character (intramolecular charge transfer state, ICT), but many details of the carotenoid to chlorophyll energy transfer mechanisms are as yet poorly understood. Here, we employ femtosecond transient absorption spectroscopy to study energy transfer pathways in the intrinsic light-harvesting complex (LHC) of dinoflagellates, which contains the carbonyl carotenoid peridinin. Carotenoid to chlorophyll energy transfer efficiency is about 90% in the 530–550 nm region, where the peridinin S₂ state transfers energy with an efficiency of 25–50%. The rest proceeds via the S₁/ICT channel, and the major S₁/ICT-mediated energy transfer pathway utilizes the relaxed S₁/ICT state and occurs with a time constant of 2.6 ps. Below 525 nm, the overall energy transfer efficiency drops because of light absorption by another carotenoid, diadinoxanthin, that contributes only marginally to energy transfer. Instead, its role is likely to be photoprotection. In addition to the peridinin-Chl-a energy transfer, it was shown that energy transfer also occurs between the two chlorophyll species in LHC, Chl-c₂ and Chl-a. The time constant characterizing the Chl-c₂ to Chl-a energy transfer is 1.4 ps. The results demonstrate that the properties of the S₁/ICT state specific for carbonyl carotenoids is the key to ensure the effective harvesting of photons in the 500–600 nm region, which is of vital importance to underwater organisms.

Marine algae are important in maintaining the stability of the Earth's biosphere because they contribute a substantial part of photosynthetic CO₂ fixation (1). An efficient light-harvesting system able to capture sunlight over a broad spectral range and transfer it to the reaction centers is a crucial part of the photosynthetic machinery. For marine photosynthetic organisms, the construction of an efficient light-harvesting system is challenging because the water functions as a filter that reduces the transmission of light in the red, and to a lesser extent in the blue, regions of the spectrum (2). Consequently, marine photosynthetic organisms have developed strategies for enhancing their light-harvesting

capacity, especially in the blue-green spectral region. Although cyanobacteria and cryptophytes use phycobiliproteins in their light-harvesting antennae to harvest blue-green light (3), marine eukaryotic algae usually employ a variety of carotenoids (peridinin, fucoxanthin, siphonaxanthin, prasinaxanthin) that contain a carbonyl group in conjugation with the carotenoid backbone (4). In contrast to higher plants, where the major light-harvesting function is performed by chlorophylls (Chl¹), carotenoids become the key light-harvesting pigments in many marine algae. Understanding carotenoid–chlorophyll energy transfer pathways is of considerable importance in understanding marine photosynthesis.

Carotenoid to (bacterio)chlorophyll energy transfer in light-harvesting complexes of higher plants and purple bacteria has been the subject of numerous experimental and theoretical studies. It is established that carotenoids are able to transfer energy from both their lowest singlet excited states, denoted S₁ and S₂, and that the overall efficiency of energy

[†] The work at Lund University was supported by grants from the Swedish Research Council and the Wallenberg Foundation. T.P. thanks the Swedish Energy Agency for supporting his stay at Lund University and the Czech Ministry of Education (grant no. MSM6007665808 and AV0Z50510513) for financial support in the Czech Republic. R.G.H. was supported by the Macquarie University Research Development Grant.

* Corresponding author. Phone: +420 389 037 561. Fax: +420 386 361 219. E-mail: polivka@ufb.jcu.cz.

[‡] University of South Bohemia.

[§] Czech Academy of Sciences.

^{||} Lund University.

[‡] Vrije Universiteit.

[#] University of California, Berkeley.

[∇] Lawrence Berkeley National Laboratory.

[○] Macquarie University.

¹ Abbreviations: Chl, chlorophyll; DDM, dodecyl maltoside; EADS, evolution-associated difference spectra; ESA, excited-state absorption; FCP, fucoxanthin-chlorophyll protein; fwhm, full width half-maximum; ICT, intramolecular charge transfer; LH2, peripheral light-harvesting complex of purple bacteria; LHC, light harvesting complex; PCP, peridinin–chlorophyll protein; SADS, species-associated difference spectra; SE, stimulated emission.

transfer varies from organism to organism (5–8). A detailed knowledge of carotenoid–chlorophyll energy transfer in marine algae is so far limited to the water-soluble peridinin–chlorophyll protein (PCP) from *Amphidinium carterae*, whose structure has been resolved to 2.0 Å resolution (9). In PCP, the ratio of peridinin to Chl-a is 4, and the energy transfer to Chl-a is via both S_2 and S_1 states with an overall efficiency close to 90% (10–14). Spectroscopic studies of both PCP and peridinin in solution reveal specific features that are assigned to the conjugated carbonyl group of peridinin. The carbonyl group introduces an additional excited state with intramolecular charge transfer (ICT) character (15–19) that is probably strongly coupled to the S_1 state (20–22). This S_1 –ICT coupling plays an important role in maintaining the high efficiency of peridinin–chlorophyll energy transfer in PCP (12, 14). Because the details of this coupling are still elusive and the decay properties of the S_1 and ICT states are not easily separable (20–24), we will, similar to previous analyses of the excited-state properties of carbonyl carotenoids in proteins (12–14, 25, 26), consider only one mixed S_1 /ICT state.

The ICT state is a common feature of all carotenoids possessing the conjugated carbonyl group (17, 21), and because these carbonyl carotenoids are important constituents of light-harvesting systems of marine algae (4), it is likely that energy transfer mechanisms observed in PCP also operate in photosynthetic antenna systems of other marine algae. Indeed, a recent study of the fucoxanthin–chlorophyll protein (FCP) from *Cyclotella meneghiniana* demonstrated that energy transfer pathways in FCP are very similar to those in PCP, although the overall efficiency of the carotenoid–chlorophyll energy transfer is lower (25). Although no other detailed time-resolved studies of energy transfer pathways in light-harvesting complexes containing carbonyl carotenoids have been reported, there are some spectroscopic observations, which attest to a high efficiency of carotenoid to chlorophyll energy transfer. For example, about 90% efficiency of energy transfer between fucoxanthin and Chl-a was reported for the FCP from *Phaeodactylum tricornutum* (27), whereas the time-resolved fluorescence spectroscopy of siphonaxanthin-containing antenna complexes suggested the efficient energy transfer between siphonaxanthin and Chl-a in the algae *Bryopsis maxima* (28) and *Codium fragile* (29).

The focus of this work is to reveal energy transfer pathways in the intrinsic light harvesting complex (LHC) from the dinoflagellate *Amphidinium carterae*. Most photosynthetic dinoflagellates have the carotenoid peridinin as the predominant carotenoid, and they possess two major types of antenna complexes: (1) the water-soluble PCP complex and (2) a membrane-bound intrinsic LHC (30–32), which, like the FCP complex, is highly homologous to the LHCI protein of higher plants (33) but exhibits a different pigment composition. In contrast to LHCI, which contains Chl-b as the accessory chlorophyll, the LHC complex from *A. carterae* utilizes Chl- c_2 (structure is shown in Supporting Information) with a Chl-a/Chl- c_2 ratio of ~ 1.7 (30). The LHC complex also has a specific carotenoid content, accommodating carotenoids, peridinin, and diadinoxanthin (see Figure 1 for structures) in a stoichiometric ratio of 5:1 (30). Thus, despite the similarity to the FCP complexes (33), it has markedly different pigment composition than the FCP complex from

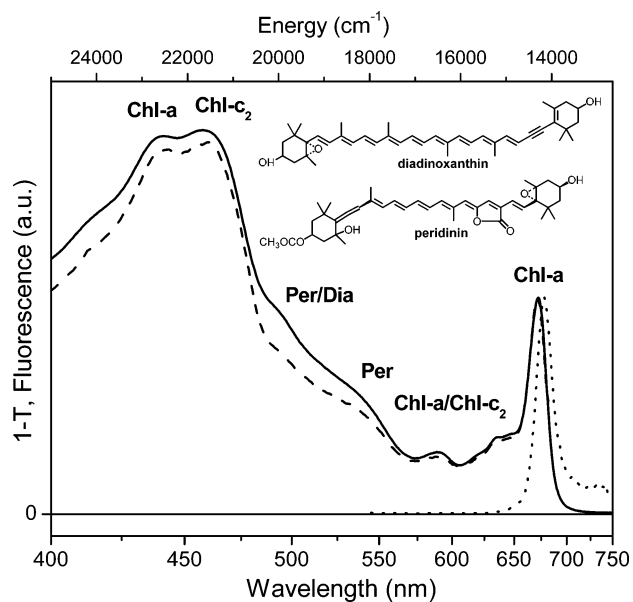


FIGURE 1: 1-T (—), fluorescence (····), and fluorescence excitation (---) spectra of the LHC. The emission spectrum was obtained after excitation at 490 nm, and the fluorescence excitation spectrum was detected at 685 nm. The structures of the two carotenoids occurring in the LHC complex are also shown.

Cyclotella meneghiniana (25, 34). Efficient energy transfer in LHC, both from carotenoid to Chl-a and from Chl- c_2 to Chl-a, was demonstrated more than a decade ago by means of fluorescence excitation spectra (30), but energy transfer pathways have not been investigated. Here, we apply femtosecond time-resolved spectroscopy in combination with global data analysis to investigate the carotenoid to chlorophyll energy transfer in the LHC. This approach, together with a comparison with the energy transfer pathways observed in other complexes, allowed us to determine the channels of energy flow within the LHC complex, and provide insight into a highly efficient light-harvesting capacity in the blue-green spectral region.

MATERIALS AND METHODS

Sample Preparation. *Amphidinium carterae* was grown under continuous illumination, harvested, and broken in a French press as described previously (35). After two washes to remove PCP and other soluble proteins, the top layer of the precipitated membranes was washed with 25 mM Tricine, 10 mM KCl at pH 7.5, and resuspended in the same buffer at a Chl-a concentration of 0.5 mg·mL⁻¹. Then, 10% β -dodecyl maltoside (β -DDM) was added to give a ratio of 40:1 w/w β -DDM to Chl-a and the solution stirred in the dark at 4 °C for 2 h. After centrifuging at 39 000g for 30 min in a Beckmann JA21 rotor, the supernatant was loaded on to a 5–40% linear sucrose gradient made in 25 mM Tricine and 10 mM KCl at pH 7.5, and centrifuged at 4 °C in a Beckman SW41 rotor at 200 000g for 18 h. An intense brown band containing the LHC was located at 5–10% sucrose. The top of the gradient together with the top 1 mm of the LHC was removed and discarded. The next 5 mm of the gradient, which contained the middle of the LHC, was collected and stored in the dark at -50 °C. Prior to the experiments, the LHC sample was thawed and dissolved in a buffer (25 mM Tris at pH 7.5, 2 mM KCl) to achieve an optical density of ~ 0.2 /mm at 500 nm. To prevent sample

degradation, all transient absorption measurements were carried out in a 2 mm quartz rotational cuvette, spinning at a frequency that ensures that the consecutive excitation pulses hit the fresh sample.

Spectroscopic Methods. Femtosecond pulses were obtained from a Ti:Sapphire oscillator, operating at a repetition rate of 82 MHz, pumped by the 5 W output of a CW frequency-doubled, diode-pumped Nd:YVO₄ laser. The pulses were amplified by a regenerative Ti:Sapphire amplifier pumped by a Nd:YLF laser (1 kHz), producing ~130 fs pulses with an average energy of ~0.9 mJ/pulse and a central wavelength at 800 nm. The amplified pulses were divided into two paths: one to pump an optical parametric amplifier for the generation of excitation pulses and the other to produce white-light continuum probe pulses in a 3 mm sapphire plate. The instrument response function varied as a function of the probing wavelength in the 130–160 fs range. The mutual polarization of the pump and probe beams was set to the magic angle (54.7°) using a polarization rotator placed in the pump beam. For signal detection, the probe beam and an identical reference beam (that had no overlap with the pump beam) were focused onto the entrance slit of a spectrograph, which then dispersed both beams onto a home-built dual photodiode array detection system. Each array contained 512 photodiodes and allowed a spectral range of ~270 nm to be measured in each laser shot. The spectral resolution of the detection system was ~80 cm⁻¹, and the energy of excitation was attenuated by neutral density filters to excitation densities varying from 3·10¹⁴ (500 and 540 nm excitation) to 6·10¹⁴ photons pulse⁻¹ cm⁻² (640 nm excitation). Absorption spectra were measured before and after measurements to ensure that no permanent photochemical changes occurred over the duration of experiment.

Data Analysis. All time-gated spectra were collated in a matrix, which was globally fitted using a sequential kinetic scheme with increasing lifetimes (36). From this, the lifetimes and the evolution-associated difference spectra (EADS) were estimated. The instrument response function (IRF) is described by a Gaussian shape, and the probe white light dispersion over the spectral range is modeled by a third order polynomial. With increasing lifetimes, the first EADS decays with the first lifetime and corresponds to the difference spectrum at time zero with an ideal infinitely short IRF. The second EADS is formed with the first lifetime and decays with the second lifetime, etc. The final EADS represents the difference spectrum of the longest living species. The error in the lifetimes obtained from the fitting procedure does not exceed 10%. EADS may not represent pure species and are interpreted as a weighted sum (with only positive contributions) of species-associated difference spectra (SADS). The quality of the fit was judged by an inspection of the singular vectors of the matrix of residuals, which had to be structureless. Next, in target analysis, a kinetic scheme was used in combination with spectral assumptions to estimate the microscopic rate constants and SADS.

RESULTS

Steady-State Spectroscopy. The 1-T (T is transmittance), emission, and fluorescence excitation spectra of the LHC complex from *A. carterae* taken at room temperature are shown in Figure 1. The main absorption features visible in

the 1-T spectrum are due to chlorophyll absorption. The Q_y band of Chl-a peaks at 672 nm. The weak bands below 660 nm are due to the Q_y bands of Chl-c₂, which were identified earlier by low-temperature absorption and circular dichroism to be located at 634 and 649 nm (30). At room temperature, the two Chl-c₂ bands are not distinguishable, and they also overlap with the higher vibrational bands of Chl-a. In the Soret region, there are two distinct absorption bands due to Chl-a (440 nm) and Chl-c₂ (458 nm). Carotenoid absorption bands overlap with the Soret bands of chlorophylls, but they also extend further to the red, filling the gap between the Soret and Q_y bands. The lowest carotenoid S₂ band located at 540 nm is assigned to peridinin, whereas the distinct shoulder at 495 nm is due to both peridinin and diadinoxanthin. This assignment of the carotenoid S₂ bands is further verified by the transient absorption data described below.

The emission spectrum of LHC excited in the carotenoid region shows a characteristic Chl-a fluorescence band peaking at 678 nm accompanied by a vibrational band at 740 nm. No hints of other emission bands have been found upon the change of excitation wavelength in the 470–550 nm region. The fluorescence excitation spectrum coincides well with the 1-T spectrum in the 550–680 nm spectral region, demonstrating nearly 100% energy transfer efficiency between Chl-c₂ and Chl-a. In the carotenoid region, the efficiency decreases. It still exceeds 90% within the lowest energy peridinin band, but drops further below 525 nm. The 495 nm shoulder attributed to diadinoxanthin is almost missing in the fluorescence excitation spectrum, indicating that this carotenoid is less involved in energy transfer as further corroborated by time-resolved measurements.

Transient-Absorption Spectroscopy in the Visible Spectral Region. The transient absorption spectra of the LHC complex measured after 540 and 500-nm excitation are depicted in Figure 2. Excitation at 540 nm (top panel) results in a transient absorption signal that resembles that observed for the PCP complex (11, 14). At 200 fs delay, the characteristic peridinin excited-state absorption (ESA) above 550 nm is a major spectral feature, accompanied by ground state bleaching below 530 nm. Even at this early time, Chl-a bleaching at 670 nm is clearly visible, consistent with an S₂-mediated energy transfer channel from peridinin to Chl-a. At longer delays, the peridinin–Chl-a energy transfer is apparent in the decay of the peridinin ESA and concomitant rise of Chl-a bleaching. At 50 ps, the transient absorption spectrum is solely due to Chl-a. The excitation of the LHC complex at 500 nm (Figure 2, middle panel) produces markedly different transient absorption spectra from those resulting from the 540-nm excitation. At 200 fs, the peridinin ESA and Chl-a bleaching dominate again, but additional bleaching below 500 nm and a new ESA band, peaking at 540 nm, appear in the transient absorption spectrum suggesting that different pigments have also been excited at 500 nm. Apparently, the excited state that gives rise to the 540-nm ESA band does not transfer energy to Chl-a because this band decays between 3 and 50 ps, but no corresponding rise of Chl-a bleaching is observed (Figure 2, middle panel). The major difference between 500 and 540 nm excitation is further demonstrated by subtracting the normalized transient absorption spectra measured at 1 ps (Figure 2, bottom panel). The difference results in a single narrow ESA band peaking at 540 nm. Both the position and width of this band match well

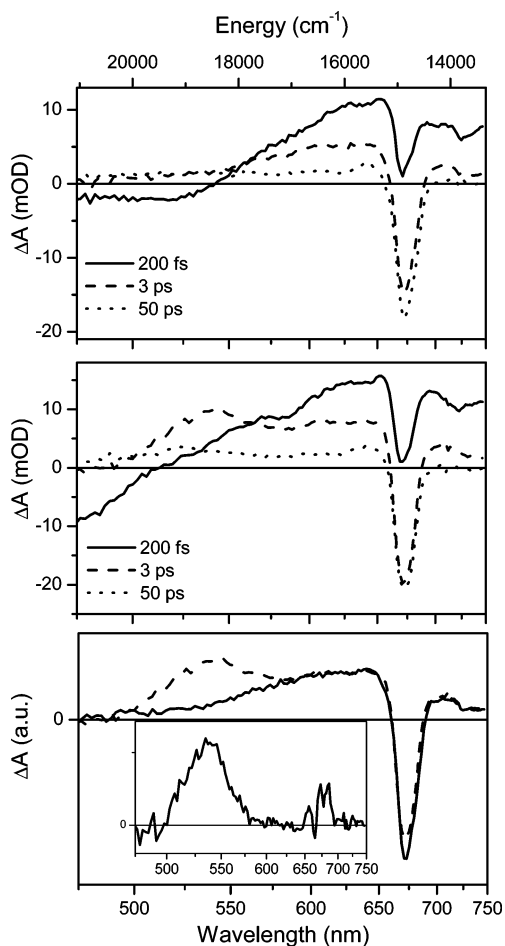


FIGURE 2: Transient absorption spectra measured at different delay times after excitation of the LHC complex at 540 nm (top) and 500 nm (middle). The bottom panel shows a comparison of transient absorption spectra taken at 1 ps after 540 nm (—) and 500 nm (---) excitations. The spectra in the bottom panel are normalized to the peridinin ESA signal at 630 nm. The difference between the two spectra is shown in the inset.

the S_1 – S_N ESA peak of violaxanthin in LHCII (37) and neurosporene in LH2 (38, 39), which have the same conjugation length as that of diadinoxanthin (5). Consequently, we assigned the 540 nm ESA band to the S_1 – S_N absorption of diadinoxanthin, which is selectively excited at 500 nm.

Global Fitting. To obtain further insight into excited-state dynamics, we have applied a global-fitting procedure to the data sets obtained after excitation at 500 and 540 nm. The resulting fits, together with the residuals demonstrating the quality of the fits at selected wavelengths, are shown in Supporting Information. In Figure 3, the results of global fitting are visualized as evolution-associated difference spectra, EADS (see the Materials and Methods section). For 540-nm excitation, at least four decay components with time constants of 0.08, 0.37, 2.6, and 15 ps are needed. In addition, one component that does not decay within the time window of our experiment (200 ps) is necessary to reproduce the equilibrated chlorophyll bleaching band that decays on the nanosecond time scale. The EADS corresponding to an excited-state species created by excitation is shown as a black line, and it exhibits typical features of the carotenoid S_2 spectrum, the ground-state bleaching below 600 nm and the excited-state absorption (ESA) because of the S_2 – S_N transi-

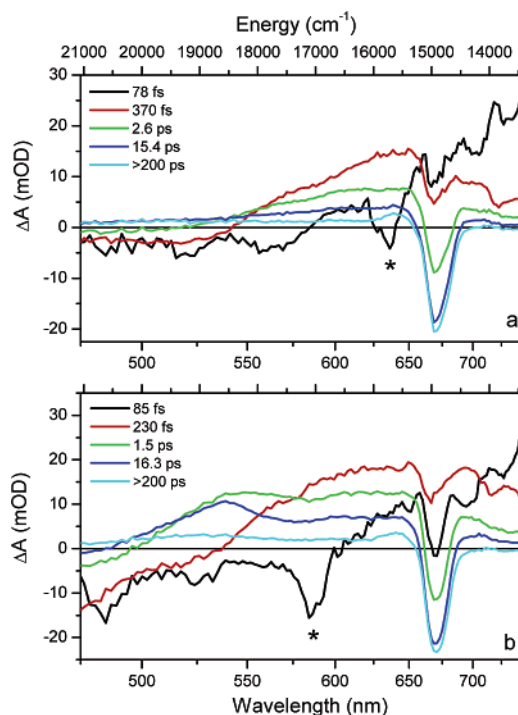


FIGURE 3: EADS resulting from the global fitting analysis of data collected after excitation at 540 nm (a) and 500 nm (b). The features marked by an asterisk are due to Raman scattering.

tion that increases toward the red. This spectrum is replaced within 80 fs by the EADS (red line), which matches a spectrum of the peridinin S_1 /ICT state well (11, 14). In addition to the peridinin S_1 /ICT ESA peaking at 630 nm and ground-state bleaching, there is a clear Chl-a bleaching appearing as a dip centered at 672 nm. The presence of Chl-a bleaching in this EADS confirms that energy transfer via the peridinin S_2 state is active in the LHC. Further dynamics occur with a time constant of 370 fs. This step is characterized by a decay of the peridinin S_1 /ICT ESA and ground-state bleaching, whereas the Chl-a bleaching becomes more pronounced, indicating energy transfer that may proceed via a hot S_1 /ICT state of peridinin (see Discussion section). Similar spectral changes also occur during further evolution of the system with a time constant of 2.6 ps, which represents energy transfer via the S_1 /ICT state of peridinin. The EADS formed during the 2.6 ps process (blue line in Figure 3) decays within 15 ps to form the EADS shown in cyan. Spectral changes during this last step are only minor and are most pronounced in the spectral region associated with the S_1 /ICT state of peridinin. This last step is most likely due to the S_1 /ICT– S_0 relaxation of peridinin molecules with less efficient energy transfer to chlorophyll (Discussion).

For 500-nm excitation, the overall evolution dynamics are comparable with those obtained after 540-nm excitation, but the spectral profiles of particular EADS are different. Again, four time constants of 0.085, 0.23, 1.5, and 16 ps, along with a nondecaying component due to the nanosecond lifetime of the final acceptor state, are needed. The first EADS formed upon excitation also contains, besides the typical peridinin S_2 state features, a hint of the Chl-a bleaching at 672 nm, signaling that a fraction of the S_2 transfer takes place within the excitation pulse. After 85 fs, this EADS is replaced by another one (red line in Figure 3b) that is clearly due to the S_1 /ICT state of peridinin. The next step occurs within 235

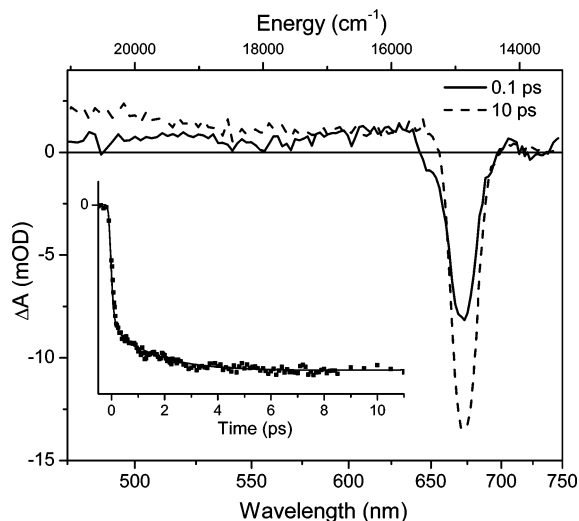


FIGURE 4: Transient absorption spectra measured at 0.1 ps (—) and 10 ps (---) after excitation of Chl- c_2 at 640 nm. The inset shows kinetics measured at 672 nm (■), together with the corresponding fit (—).

fs and is characterized by two major processes. First, the Chl-*a* bleaching increases significantly, indicating peridinin to Chl-*a* energy transfer. Second, a new band at 540 nm appears, most likely resulting from the population of the S_1 state of diadinoxanthin. This EADS decays within 1.5 ps, and this evolution is again dominated by an increase of Chl-*a* bleaching and a decay of the S_1 /ICT state of peridinin. The 540 nm band, which is presumably due to the S_1 - S_N transition of diadinoxanthin, does not decay during this step. Later, however, the 540-nm band disappears during the 16 ps time evolution. The disappearance of the 540-nm band is not accompanied by a corresponding rise of Chl-*a* bleaching, indicating that the decay of this band is due to S_1 - S_0 relaxation of diadinoxanthin rather than energy transfer.

Besides the carotenoid-Chl-*a* energy transfer, the presence of two chlorophyll species suggest the possibility of Chl- c_2 to Chl-*a* energy transfer. To explore the Chl-Chl energy transfer, the LHC complex was excited into the Chl- c_2 Q_y band at 640 nm. The resulting transient absorption spectra recorded at 100 fs and 10 ps are shown in Figure 4. At 100-fs delay, a weak negative shoulder at 645 nm due to Chl- c_2 bleaching is present, together with a main negative band due to Chl-*a* bleaching centered at 672 nm. The Chl- c_2 bleaching disappears, whereas the Chl-*a* band rises even further on the picosecond time scale (Figure 4, inset). Global fitting reveals two main time components of 75 fs and 1.4 ps.

Transient Absorption Spectroscopy in the Near-IR Region.

In the spectral region from 550 to 700 nm, the LHC transient absorption profile is similar to that of peridinin in a polar environment, suggesting the formation of the S_1 /ICT state with significant charge-transfer character (17, 21, 22). To explore the possibility that this state is populated in LHCs, transient absorption spectra and kinetics were recorded in the 800–1000 nm region, where the ICT stimulated emission is observed (18). Results following 540-nm excitation are depicted in Figure 5. The transient absorption spectrum recorded at 0.3 ps after excitation has a weak negative band at around 930 nm that is consistent with the ICT stimulated emission observed for the PCP complex (12). This assign-

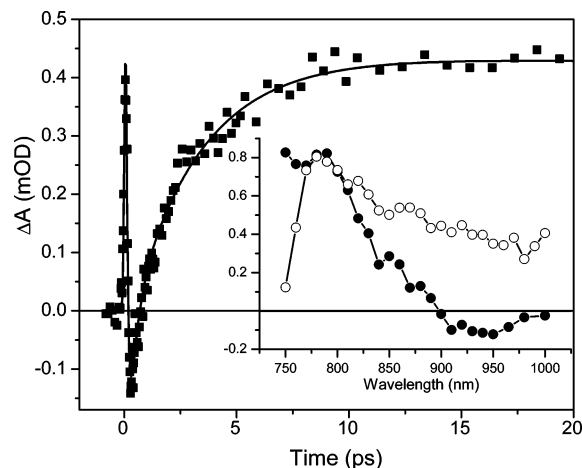


FIGURE 5: Kinetics measured at 930 nm after excitation of the LHC at 540 nm. The solid line (—) represents the best fit of the data. Inset: transient absorption spectra measured at 0.3 ps (●) and 10 ps (○) after excitation at 540 nm.

ment is supported by the kinetics recorded at 930 nm. An initial positive signal is due to the S_2 - S_N ESA of peridinin, which decays with a 70 fs time constant to form the negative signal characteristic of the ICT stimulated emission. The ICT stimulated emission decays with a major component of 3 ps. The fit is improved with an additional decay component of 0.35 ps. The final positive signal at 10 ps is due to Chl-*a* ESA that does not decay within the time of the experiment (spectral profiles are shown in the inset in Figure 5). The time constants extracted from the fitting of the 930-nm kinetics match closely those obtained from the global fitting of the transient absorption spectra in the visible spectral region, indicating that in the LHC as in the PCP complex (12) the S_1 /ICT state of peridinin actively participates in the peridinin to Chl-*a* energy transfer.

DISCUSSION

The results presented in the previous section demonstrate the efficient energy transfer among pigments in the LHC from *A. carterae*. The energy transfer efficiency varies within the 400–600 nm spectral region, indicating different energy transfer efficiencies for individual carotenoids in the LHC complex. Consequently, the network of energy transfer pathways is expected to be complex and its elucidation hindered by an unknown structure of this complex and a debatable exact pigment composition. The originally proposed number of pigments of 7 Chl-*a*, 4 Chl- c_2 , 10 peridinins, and 2 diadinoxanthins per LHC subunit (30) seems to be unrealistically high compared with those of the closely related FCP (33, 34) or LHCII (40). Moreover, unlike the LHCII, whose Chl-*a* Q_y band is shifted to ~680 nm due to excitonic interactions, in LHC, no such shift is observed, indicating that chlorophylls are likely to be less closely packed (8). It is possible that the actual number of pigments per LHC subunit is less than originally suggested. Recently, a similar conclusion was reached for the FCP complex (25).

The expected complexity of the energy transfer pathways implies that although the sequential model used for the fitting of the data in the Results section (Figure 4) provides important information about the time evolution of the system, it cannot truly reproduce the spectra of the individual excited states involved in energy transfer. Therefore, a target analysis

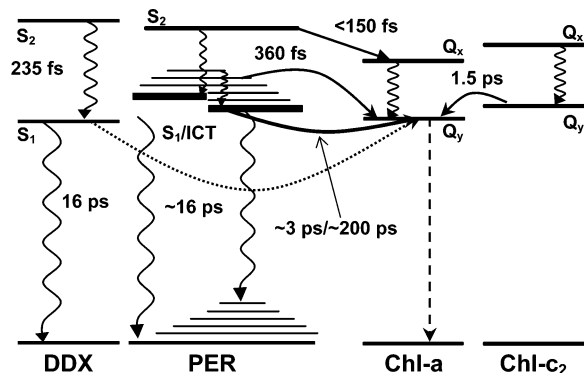


FIGURE 6: Schematic representation of the model describing energy transfer pathways within the LHC complex. The solid arrows depict the main energy transfer channels, whereas the dotted arrow indicates the possible minor energy transfer pathway from diadinoxanthin to Chl-a. Wavy arrows represent nonradiative relaxation processes, and the dashed arrow corresponds to the fluorescence of the lowest-lying Chl-a. See text for details.

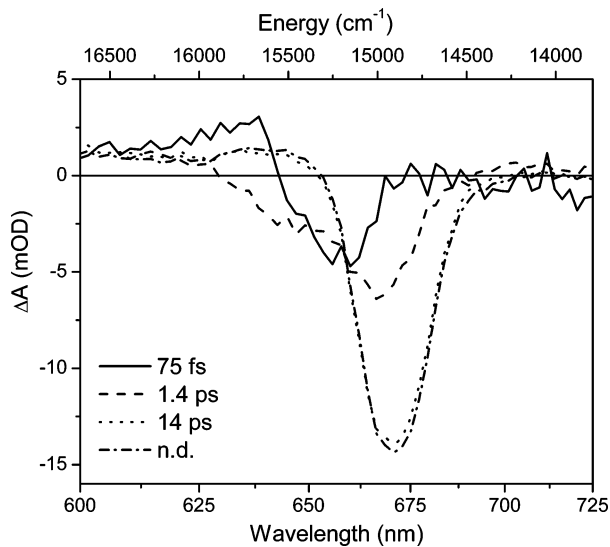


FIGURE 7: SADS resulting from the target analysis of the data obtained after Chl-c₂ excitation at 640 nm.

aiming for a specific model of energy transfer pathways is needed (36). To describe the experimental data, we have constructed a model, which is depicted in Figure 6. To simplify the scheme, both Chl-a and peridinin are each represented only by one molecule, although it is obvious from pigment composition that more than one spectral form may be present for these pigments. The target analysis indeed revealed that the peridinin in the scheme represents at least two distinct types of peridinin molecules, each transferring energy via their S₁/ICT states with different efficiencies (see below). The species-associated difference spectra (SADS) corresponding to individual excited-state species that result from the fitting of the data obtained after excitation of Chl-c₂ at 640 nm are displayed in Figure 7. For the excitation in the carotenoid region, the experimental data obtained for 500 and 540 nm excitation were fitted simultaneously to the model, and the resulting SADS are shown in Figure 8. In the following, we will discuss the network of the energy transfer pathways according to the model presented in Figure 6 and the EADS and SADS shown in Figures 4, 7, and 8.

Chl-c₂ to Chl-a Energy Transfer. To explore the dynamics of energy transfer between chlorophylls, we have first performed the target analysis of the data obtained after

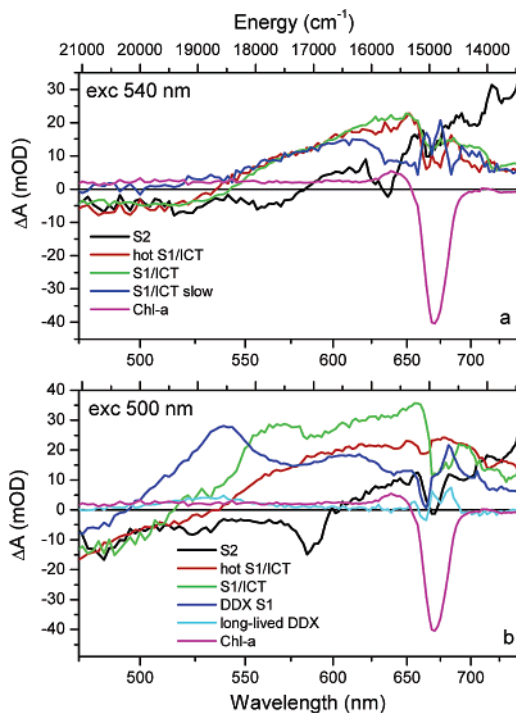


FIGURE 8: SADS resulting from the simultaneous target analysis of data obtained after 500 and 540 nm excitations using the kinetic scheme depicted in Figure 6. The resulting SADS corresponding to the species formed after either the 540 or the 500 nm excitation are shown in the top and bottom panels, respectively. See text for details.

excitation of Chl-c₂ at 640 nm. The initial SADS contains a bleaching signal peaking at 655 nm. The apparent red shift of Chl-c₂ bleaching is probably caused by an overlap with the ESA signal in the 620–640 nm region and/or a contribution from a coherent artifact in the transient absorption spectra around time zero. Partial excitation of the Chl-a via the higher vibrational bands also contribute to this spectrum. This SADS decays in 75 fs via two channels. One channel (40%) forms a species characterized by the SADS (dashed line in Figure 7) that contain both Chl-c₂ and Chl-a bleaching. The presence of an ultrafast blue-shifted (665 nm) Chl-a bleach is likely due to the direct excitation of the blue Chl-a population followed by further Chl-a equilibration. This species containing contributions from both Chl-c₂ and Chl-a evolves in 1.4 ps to form a pure Chl-a spectrum (dash-dot line), indicating that the 1.4 ps process characterizes the Chl-c₂ to Chl-a energy transfer. The rest (60%) of the initially excited population forms a spectrum shown as a dotted line in Figure 7, which is clearly due to Chl-a. A major part of this process most likely reflects relaxation among Chl-a molecules excited directly into higher vibrational bands by the 640-nm excitation. However, as the contribution of direct excitation of Chl-a at 640 nm is less than 60%, it indicates that some fraction of the Chl-c₂ to Chl-a energy transfer also proceeds on a sub-100 fs time scale. The Chl-a spectrum exhibits a slight equilibration displayed as a subtle red shift taking place at a 14 ps time scale (evolution from the dotted to the dash-dotted spectrum in Figure 7) that resembles a Chl-a equilibration process observed in the LHCI antenna (41).

Energy Transfer via the Carotenoid S₂ State. When excited to the carotenoid region, the initial EADS corresponding to the excited-state species formed by the excitation pulse

includes weak Chl-a bleaching, indicating that the S_2 channel is active. The efficiency of the S_2 transfer depends on excitation wavelength. Although the peridinin molecules excited at 540 nm exhibit rather weak Chl-a bleaching in the first EADS, the S_2 pathway becomes more active when the excitation wavelength is moved to 500 nm. This is evidenced by significant Chl-a bleaching in the first EADS in Figure 3b, signaling that a substantial fraction of the S_2 population transfers energy to Chl-a. In addition, a small fraction of Chl-c₂ may be involved because the red tail of the Chl-c₂ Soret band may be excited at 500 nm. The increase in efficiency of the S_2 channel is not due to diadinoxanthin, which is selectively excited at 500 nm, because the 540-nm band characteristic of the diadinoxanthin S_1 state does not appear until the third EADS formed with a 230 fs time constant, which is consequently assigned to the S_2 lifetime of diadinoxanthin in the LHC complex. Thus, diadinoxanthin cannot be a donor in the efficient S_2 -mediated energy transfer because the S_2 lifetime of the donor must be shorter than the lifetime of the first EADS, 85 fs. Consequently, the S_2 pathway is operated exclusively by peridinin. For the 540-nm excitation, only peridinin is excited, and the fraction of the Chl-a bleaching signal formed during the first step is characterized by a 78 fs time constant. The peridinin S_2 lifetimes of 78 fs (excitation at 540 nm) and <85 fs (excitation at 500 nm) can, in principle, be used for the calculation of the efficiency of the S_2 -mediated energy transfer from peridinin to Chl-a. But because these values are beyond the limits of our time resolution and because there is no clear consensus concerning the intrinsic (in the absence of energy transfer) peridinin S_2 lifetime as values of 55–130 fs have been reported (13, 20, 22), a detailed quantitative analysis is impossible. On the basis of the above-mentioned values and the magnitude of the initial Chl-a bleaching observed in EADS, we can estimate that the peridinin S_2 state in the LHC transfers energy to Chl-a with an efficiency of 25–50%.

Energy Transfer via the S_1 /ICT State. Despite the active S_2 channel, a substantial part of the carotenoid–chlorophyll energy transfer proceeds via the S_1 /ICT channel as in the PCP complex (10–14). Both the spectral shape of the S_1 /ICT band (Figure 8) and the stimulated emission in the near-infrared region (Figure 5) show that the S_1 /ICT state has substantial ICT character. The EADS shown in Figure 3 demonstrate that the S_1 /ICT energy transfer in the LHC complex includes three separate processes characterized by time constants of 370 fs, 2.6 ps, and 15 ps for 540 nm excitation and 230 fs, 1.5 ps, and 16 ps for 500 nm excitation. This situation is somewhat reminiscent of that observed for the PCP complex (11, 12–14), but a closer look reveals significant differences between the LHC and PCP complexes.

The fastest process can, as in PCP, be attributed to energy transfer via the hot S_1 /ICT state. In PCP, this channel was found to be of minor importance and proceeded with a 0.7 ps time constant (12, 13), but the LHC complex utilizes this channel with significantly higher efficiency. The high efficiency of this pathway is obvious from the EADS shown in Figure 3a; during the 370 fs step, Chl-a bleaching substantially increases, making this channel comparable in efficiency with that of the transfer via the relaxed S_1 /ICT state. The same is valid for the 230 fs step that is observed after 500-nm excitation (Figure 3b). The excitation wave-

length dependence may be due to the excitation of diadinoxanthin at 500 nm whose S_2 – S_1 relaxation adds to the relaxation pattern. The shorter lifetime of 230 fs for the hot S_1 /ICT channel after 500-nm excitation, thus, may result from the mixing of time constants for the S_2 lifetime of diadinoxanthin and the true lifetime of the hot S_1 /ICT state of peridinin. Consequently, the 370 fs process following excitation at 540 nm is probably the correct value associated with energy transfer via the hot S_1 /ICT channel.

Because the fitted SADS corresponding to the hot S_1 /ICT and relaxed S_1 /ICT states are quite similar, especially after 540-nm excitation (Figure 8), it could be argued that a separate hot S_1 /ICT state is not necessary to explain the data. Energy transfer via a relaxed S_1 /ICT state of a peridinin molecule having a particularly favorable orientation with respect to Chl-a might also proceed more rapidly. This is a plausible interpretation of the data because the LHC complex accommodates more Chl acceptors than PCP, increasing the number of possible orientations. Assuming the same intrinsic (without energy transfer) peridinin S_1 /ICT lifetime in the LHC as that in PCP (~16 ps), (12, 14) the efficiency of the S_1 /ICT channel would be 98%. Whichever interpretation is valid, this channel represents a significant contribution to the overall peridinin–chlorophyll energy transfer.

The 2.6 ps process is clearly due to energy transfer via the relaxed S_1 /ICT state of peridinin. This assignment is also apparent from a direct comparison of the Chl-a rise and S_1 /ICT decay of peridinin in the LHC and PCP (Figure 9), where this energy transfer represents the dominating energy transfer pathway. In LHCs, the lifetime of this relaxed S_1 /ICT state varies with excitation wavelength, changing from 2.6 ps (540-nm excitation) to 1.5 ps (500-nm excitation). The origin of this difference is unclear, although a plausible explanation may be that the peridinin molecule predominantly excited at 500 nm exhibits more efficient S_1 /ICT transfer. Another explanation could be that the SADS attributed to the relaxed S_1 /ICT state in Figure 8b is not pure S_1 /ICT spectrum of peridinin but contains some contribution from diadinoxanthin excited at 500 nm. Such a contribution may be traced in the peculiar shape of the S_1 /ICT spectrum, which contains a clear shoulder at 570 nm that is not characteristic of the peridinin S_1 /ICT state (20–22). It is worth noticing that this shoulder is red-shifted as compared to the S_1 state of diadinoxanthin (blue SADS in Figure 8) and may, thus, be due to a contribution from a hot vibrational S_1 state of diadinoxanthin. Because the S_1 vibrational relaxation in noncarbonyl carotenoids occurs on 300–800 fs time scales (42, 43), such mixing would also lead to the apparent shortening of the peridinin S_1 /ICT lifetime observed after the 500 nm excitation. Clearly, further studies utilizing a wider range of excitation wavelengths and/or other experimental approaches are required to clarify this issue.

The 15 ps process in the LHC also has a counterpart in the PCP complex. In PCP, it was attributed to the equilibration/annihilation between chlorophylls or to the S_1 /ICT decay of a peridinin molecule that does not transfer energy to Chl (11, 12, 14). In the LHC, however, this process must be associated with energy transfer because there is a clear increase of the Chl-a bleaching signal during the 15 ps step (Figure 3). Its SADS resemble the characteristic profile of the peridinin S_1 /ICT state; therefore, we attributed it to energy transfer from the relaxed S_1 /ICT state of one (or more)

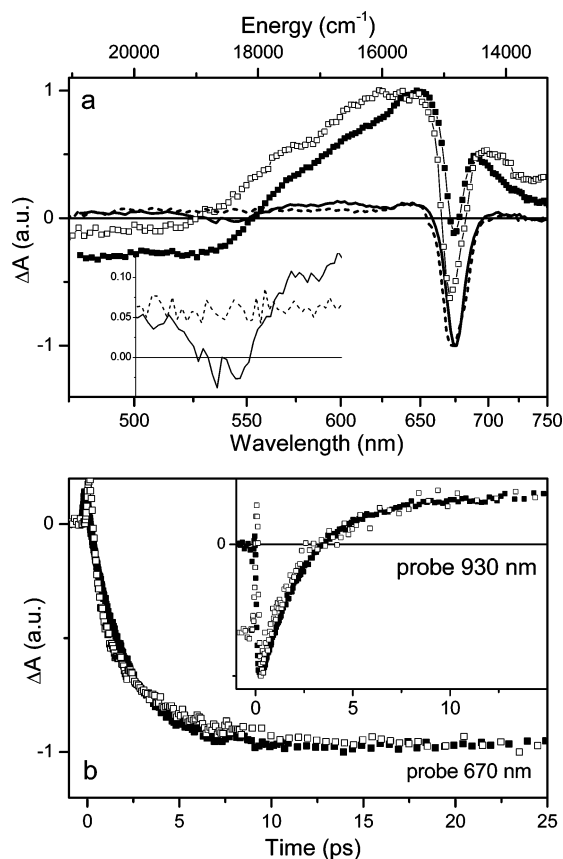


FIGURE 9: Comparison of excited-state dynamics in the LHC and PCP complexes from *A. carterae*. (a) Transient absorption spectra taken at 0.5 ps for LHC (□) and PCP (■) after excitation at 540 nm. Transient absorption spectra corresponding to Chl-a ESA taken at 10 ps are also shown (—, PCP; ----, LHC). Inset: enlargement of the y-axis for the Chl-a ESA signals at 10 ps in the 500–600 nm spectral region. (b) Kinetics of Chl-a rise probed at 675 nm for PCP (■) and at 672 nm for LHC (□) after excitation at 540 nm. Inset: kinetics probed at 930 nm for LHC (□) and PCP (■). To emphasize the similarity of the decays, the vertical offset is introduced for the LHC complex kinetics to compensate for the strong Chl-a ESA in the LHC. All kinetics are normalized to their minima.

peridinin molecule that has only a weak coupling to Chl-a. The efficiency of this channel is only ~6%, assuming the intrinsic peridinin lifetime of 16 ps leading to the energy transfer time of ~200 ps (Figure 6).

Role of Diadinoxanthin. When the excitation wavelength is shifted to 500 nm, the other carotenoid, diadinoxanthin, is also excited as indicated by a distinct spectral band in the transient absorption spectra located at 540 nm. Interestingly, the data presented here suggests that diadinoxanthin is only a little (if at all) involved in carotenoid–chlorophyll energy transfer. The diadinoxanthin S_2 lifetime of ~230 fs, obtained from the rise of the 540-nm band, is in the range obtained for carotenoids of similar conjugation length in solution (5), indicating an inactive S_2 -channel. The S_1 lifetime of 16 ps may point to an involvement in energy transfer because the S_1 lifetime of diadinoxanthin in solution is 23 ps (44), and EADS shown in Figure 3b exhibit a slight increase of the Chl-a bleaching during the 16-ps step. If this were the case, the efficiency of S_1 -mediated energy transfer via diadinoxanthin would be ~30%. However, the SADS corresponding to the S_1 state of diadinoxanthin contains, besides the narrow 540-nm band, a red tail resembling the S_1 /ICT state of

peridinin (Figure 8b). Because diadinoxanthin has no conjugated carbonyl group, its S_1 state should exhibit only a narrow S_1 – S_N ESA (17). Hence, the resulting SADS is probably a mixture of the diadinoxanthin S_1 state and a ‘15-ps peridinin’ S_1 /ICT state. The increase in Chl-a bleaching during the 16-ps time evolution also may be due to energy transfer from a slowly transferring peridinin, as in the case of 540-nm excitation. In this case, the shorter S_1 lifetime of diadinoxanthin must be due to the specific interaction with the protein, a situation observed earlier for carotenoids in reconstituted LHCII complexes (37) and in other carotenoid-binding proteins (26, 45). Although it is impossible to precisely evaluate the involvement of the S_1 state of diadinoxanthin in energy transfer, we concluded that the upper limit for the diadinoxanthin–chlorophyll energy transfer efficiency is 30%, which, taking into account the 5:1 peridinin/diadinoxanthin ratio, makes the diadinoxanthin contribution to the overall carotenoid–chlorophyll energy transfer in the LHC negligible. In addition, target analysis revealed a weak long-lived band around 530 nm (Figure 8). Because this band is observed exclusively after 500-nm excitation, it is probably related to diadinoxanthin. The origin of this band cannot be precisely determined, but it may be either due to a triplet state formed by an ultrafast channel similar to that observed in bacterial light-harvesting complexes (46) or due to other long-lived excited states that were recently observed for some carotenoids (47).

What then is the major role of diadinoxanthin in the LHC complex? Diadinoxanthin has been shown to be involved in photoprotection in algae. Johnsen et al. showed that under high-light conditions the diadinoxanthin content in certain red tide dinoflagellates exhibits an increase that is accompanied by a decrease of the fluorescence yield (48). Many species of algae utilize an alternative xanthophyll cycle that involves the interconversion of the carotenoids diadinoxanthin and diatoxanthin (44), and changes in diadinoxanthin/diatoxanthin ratio have been correlated with irradiance levels during algal growth (49). In this modified xanthophyll cycle, high-light conditions promote the conversion of diadinoxanthin to diatoxanthin and may lead to the direct quenching of chlorophyll fluorescence by energy transfer to the S_1 state of diatoxanthin (44) or by a charge separation as recently shown for higher plants (50). Thus, there is indication that diadinoxanthin is involved in photoprotective actions in algae, and by direct analogy with the LHCII complex (40, 51), there may be a quenching site occupied by diadinoxanthin in the *Amphidinium* LHC.

Comparison of LHC, PCP and FCP. All these light-harvesting complexes utilize carbonyl carotenoids, and it is, therefore, useful to compare the energy transfer dynamics of these three complexes. The LHC and PCP complexes both utilize peridinin, which has the most pronounced polarity driven behavior of all carbonyl carotenoids. From the spectroscopic point of view, there are three major differences between the LHC and PCP. First, the different protein environments and presumably more peridinin molecules in the LHC complex make the spectrum of the S_1 /ICT ESA broader than that in the PCP complex (Figure 9a), which could be attributed to larger spectral heterogeneity in LHC. Second, the Chl-a SADS in the LHC complex lack the peridinin response, which in PCP is a pronounced negative band around 530 nm (see inset of Figure 9a), indicating a

weaker electrostatic interaction between Chl and peridinin in the LHC. The lack of carotenoid response was also observed in FCP (25). Third, although in the PCP complex the efficiency of peridinin–chlorophyll energy transfer is uniform across the whole peridinin absorption band (52), certain variability in carotenoid–chlorophyll energy transfer efficiency is observed for the LHC complex (Figure 1). This is caused by the presence of diadinoxanthin, which exhibits very low energy transfer efficiency, causing the drop in energy transfer efficiency below 525 nm (Figure 1).

When peridinin is excited at 540 nm, pathways and efficiencies of peridinin–chlorophyll energy transfer are quite similar in LHC and PCP. In both complexes, the S_2 channel is active with an efficiency in the 25–50% range. The S_1 /ICT lifetimes of peridinin in both complexes are nearly identical (Figure 9b). Moreover, the same S_1 /ICT lifetime of 2.5 ps was also obtained after 530-nm excitation of fucoxanthin in the FCP complex (25). Because the intrinsic lifetimes of these carbonyl carotenoids vary with polarity (17, 21), it suggests that the polarity of the environment in all of these complexes is tuned in a similar way to obtain maximal efficiency of the carotenoid–chlorophyll energy transfer in the 500–600 nm spectral region. In the LHC complex, the ability to absorb photons accessible to aquatic organisms is further enhanced by the presence of Chl- c_2 , which covers the 600–640 nm region. The effective utilization of light in this spectral region is achieved by the highly efficient Chl- c_2 to Chl-a energy transfer (Figures 1, 7, and S_1). The same situation occurs in the FCP complex (25).

In summary, our results show that the intrinsic LHC complex from *A. carterae* exhibits an efficient peridinin–Chl energy transfer that utilizes both S_2 and S_1 /ICT channels with efficiencies varying with excitation wavelength. It must be noted, however, that global analysis showed that energy transfer via the S_1 /ICT state proceeds via at least three channels. Only one of these channels, characterized by a 2.5 ps time constant, could be safely assigned to the energy transfer via the relaxed S_1 /ICT state. The other S_1 /ICT mediated channels may involve a hot S_1 /ICT state and/or peridinin molecules having different coupling to Chl-a. Similarly, disentangling the intricate network of energy transfer pathways occurring after 500 nm excitation is complicated because additional relaxation processes created by the excitation of the other carotenoid, diadinoxanthin (such as S_1 vibrational relaxation), make it unfeasible to include all possible processes that take place at similar time scales into data analysis. Finally, it should also be mentioned that we did not include the peridinin to Chl- c_2 pathway into our analysis. This pathway may, in principle, be active from both S_2 and S_1 /ICT states of peridinin, but because of the fast energy transfer from Chl- c_2 to Chl-a and because of the rather weak spectral signs of Chl- c_2 , it was not possible to make any conclusions about this energy transfer channel. Despite all these complications whose solution awaits further studies, we can safely conclude that peridinin is the main light-harvesting carotenoid in the LHC and transfers energy from both S_2 and S_1 /ICT states. The total energy transfer efficiency is maximal in the 530–550 nm region (~90% on the basis of fluorescence excitation spectra), with about 25–50% proceeding via the S_2 channel. Below 520 nm, the overall efficiency drops because of the presence of the carotenoid, diadinoxanthin, whose involvement in energy

transfer is only marginal. The role of diadinoxanthin in the LHC is most likely photoprotection. Besides the efficient peridinin–Chl-a energy transfer, the light-harvesting capacity of the LHC complex is further enhanced by the nearly 100% efficient Chl- c_2 to Chl-a energy transfer. The results on the LHC complex also confirm the specific light-harvesting strategy developed by marine algae. The antenna systems of marine algae contain pigments that effectively harvest photons in the 500–600 nm region where the under-water spectral distribution of irradiance has a maximum (2). To optimize light-harvesting capacity in this spectral region, these organisms exploit carbonyl carotenoids. The strong polarity dependence of the spectroscopic properties of these carotenoids allows for the optimal tuning of carotenoid photophysical properties by the interaction with protein, which ensures both effective absorption in the 500–600 nm region and highly efficient carotenoid–chlorophyll energy transfer.

ACKNOWLEDGMENT

We thank Frank Sharples for help with LHC isolation and purification and Özlem İpek and Aleš Holoubek for assistance with measurements of fluorescence and fluorescence excitation spectra.

SUPPORTING INFORMATION AVAILABLE

Comparison of global fitting results and raw data and structures of Chl- c_2 and Chl-a. This material is available free of charge via the Internet at <http://pubs.acs.org>.

REFERENCES

- Hiller, R. G. (1999) Carotenoids as components of the light-harvesting proteins of eucaryotic algae, in *Photochemistry of Carotenoids* (Frank, H. A., Young, A. J., Britton, G. Cogdell, R. J., Eds.) Dordrecht, The Netherlands, pp 81–98.
- Borrego, C. M., Garcia-Gil, L. J., Vila, X., Cristina, X. P., Figueras, J. B., and Abella, C. A. (1997) Distribution of bacteriochlorophyll homologs in natural populations of brown-colored phototrophic sulfur bacteria, *FEMS Microbiol. Ecol.* 24, 301–309.
- Glazer, A. N. (1984) Phycobilisome: a macromolecular complex optimized for light energy transfer, *Biochim. Biophys. Acta* 768, 29–51.
- Macpherson, A. N., and Hiller, R. G. (2003) Light-harvesting systems in chlorophyll c-containing algae, in *Light-Harvesting Antennas in Photosynthesis* (Green, R. B., Parson, W. W., Eds.) Dordrecht, The Netherlands.
- Polívka, T., and Sundström, V. (2004) Ultrafast dynamics of carotenoid excited states. From solution to natural and artificial systems, *Chem. Rev.* 104, 2021–2071.
- Frank, H. A., and Cogdell, R. J. (1996) Carotenoids in photosynthesis, *Photochem. Photobiol.* 63, 257–264.
- Ritz, T., Damjanović, A., Schulten, K., Zhang, J.-P., and Koyama, Y. (2000) Efficient light harvesting through carotenoids, *Photosynth. Res.* 66, 125–144.
- van Amerongen, H., and van Grondelle, R. (2001) Understanding the energy transfer function of LHCII, the major light-harvesting complex of green plants, *J. Phys. Chem. B* 105, 604–617.
- Hofmann, E., Wrench, P., Sharples, F. P., Hiller, R. G., Welte, W., and Diederichs, K. (1996) Structural basis of light harvesting by carotenoids: Peridinin-chlorophyll-protein from *Amphidinium carterae*, *Science* 272, 1788–1791.
- Bautista, J. A., Hiller, R. G., Sharples, F. P., Gosztola, D., Wasielewski, M., and Frank, H. A. (1999) Singlet and triplet energy transfer in the peridinin–chlorophyll a protein from *Amphidinium carterae*, *J. Phys. Chem. A* 103, 2267–2273.
- Krueger, B. P., Lampoura, S. S., van Stokkum, I. H. M., Papagiannakis, E., Salverda, J. M., Gradinaru, C. C., Rutkauskas, D., Hiller, R. G., and van Grondelle, R. (2001) Energy transfer in the peridinin chlorophyll-a protein of *Amphidinium carterae*

- studied by polarized transient absorption and target analysis, *Biophys. J.* **80**, 2843–2855.
12. Zigmantas, D., Hiller, R. G., Sundström, V., and Polívka, T. (2002) Carotenoid to chlorophyll energy transfer in the peridinin-chlorophyll-a-protein complex involves an intramolecular charge transfer state, *Proc. Natl. Acad. Sci. U.S.A.* **99**, 16760–16765.
 13. Linden, P. A., Zimmermann, J., Brixner T, Holt, N. E., Vaswani, H., Hiller, R. G., and Fleming, G. R. (2004) Transient absorption study of peridinin and peridinin-chlorophyll-a-protein after two photon excitation, *J. Phys. Chem. B* **108**, 10340–10345.
 14. Polívka, T., Pascher, T., Sundström, V., and Hiller, R. G. (2005) Tuning energy transfer in the peridinin-chlorophyll complex by reconstitution with different chlorophylls, *Photosynth. Res.* **86**, 217–227.
 15. Bautista, J. A., Connors, R. E., Raju, B. B., Hiller, R. G., Sharples, F. P., Gosztola, D., Wasielewski, M. R., and Frank, H. A. (1999) Excited-state properties of peridinin: Observation of a solvent dependence of the lowest excited singlet state lifetime and spectral behavior unique among carotenoids, *J. Phys. Chem. B* **103**, 8751–8758.
 16. Premvardhan, L., Papagiannakis, E., Hiller, R. G., and van Grondelle, R. (2005) The charge-transfer character of the S_0 – S_2 transition in the carotenoid peridinin is revealed by Stark spectroscopy, *J. Phys. Chem. B* **109**, 15589–15597.
 17. Frank, H. A., Bautista, J. A., Josue, J., Pendon, Z., Hiller, R. G., Sharples, F. P., Gosztola, D., and Wasielewski, M. R. (2000) Effect of the solvent environment on the spectroscopic properties and dynamics of the lowest excited states of carotenoids, *J. Phys. Chem. B* **104**, 4569–4577.
 18. Zigmantas, D., Polívka, T., Hiller, R. G., Yartsev, A., and Sundström, V. (2001) Spectroscopic and dynamic properties of the peridinin lowest singlet excited states, *J. Phys. Chem. A* **105**, 10296–10306.
 19. Vaswani, H. M., Hsu, C.-P., Head-Gordon, M.P., and Fleming, G. R. (2003) Quantum mechanical evidence for an intramolecular charge-transfer state in the carotenoid peridinin of peridinin-chlorophyll-protein, *J. Phys. Chem. B* **107**, 7940–7946.
 20. Zigmantas, D., Hiller, R. G., Yartsev, A., Sundström, V., and Polívka, T. (2003) Dynamics of excited states of the carotenoid peridinin in polar solvents: Dependence on excitation wavelength, viscosity, and temperature, *J. Phys. Chem B* **107**, 5339–5348.
 21. Zigmantas, D., Hiller, R. G., Sharples, F. P., Frank, H. A., Sundström, V., and Polívka, T. (2004) Effect of a conjugated carbonyl group on the photophysical properties of carotenoids, *Phys. Chem. Chem. Phys.* **6**, 3009–3016.
 22. Papagiannakis, E., Larsen, D. S., van Stokkum, I. H. M., Vengris, M., Hiller, R. G., and van Grondelle, R. (2004) Resolving the excited-state equilibrium of peridinin in solution, *Biochemistry* **43**, 15303–15309.
 23. Shima, S., Ilagan, R. P., Gillespie, N., Sommer, B. J., Hiller, R. G., Sharples, F. P., Frank, H. A., and Birge, R. R. (2003) Two-photon and fluorescence spectroscopy and the effect of environment on the photochemical properties of peridinin in solution and in the peridinin-chlorophyll-protein from *Amphidinium carterae*, *J. Phys. Chem. A* **107**, 8052–8066.
 24. Papagiannakis, E., Vengris, M., Larsen, D. S., Van Stokkum, I. H. M., Hiller, R. G., and van Grondelle, R. (2006) Use of ultrafast dispersed pump-dump-probe and pump-repump-probe spectroscopies to explore the light-induced dynamics of peridinin in solution, *J. Phys. Chem. B* **110**, 512–521.
 25. Papagiannakis, E., van Stokkum, I. H. M., Fey, H., Büchel, C., and van Grondelle, R. (2005) Spectroscopic characterization of the excitation energy transfer in the fucoxanthin-chlorophyll protein of diatoms, *Photosynth. Res.* **86**, 241–250.
 26. Polívka, T., Kerfeld, C. A., Pascher, T., and Sundström, V. (2005) Spectroscopic properties of the carotenoid 3'-hydroxyechinenone in the orange carotenoid protein from the cyanobacterium *Arthrospira maxima*, *Biochemistry* **44**, 3994–4003.
 27. Trautman, J. K., Shreve, A. P., Owens, T. G., and Albrecht A. C. (1990) Femtosecond dynamics of carotenoid-to-chlorophyll energy transfer in thylakoid membrane preparations from *Phaeodactylum tricorutum* and *Nannochloropsis* sp., *Chem. Phys. Lett.* **166**, 369–374.
 28. Nakayama, K., Mimuro, M., Nishimura, Y., Yamazaki, I., and Okada, M. (1994) Kinetic analysis of energy transfer processes in LHC isolated from the siphonous green alga *Bryopsis maxima* with use of picosecond fluorescence spectroscopy, *Biochim. Biophys. Acta* **1188**, 117–124.
 29. Akimoto, S., Yamazaki, I., Murakami, A., Takaichi, S. and Mimuro, M. (2004) Ultrafast excitation relaxation dynamics and energy transfer in the siphonoxanthin-containing green alga *Codium fragile*, *Chem. Phys. Lett.* **390**, 45–49.
 30. Hiller, R. G., Wrench, P. M., Gooley, A. P., Shoebridge, G. and Breton, J. (1993) The major intrinsic light-harvesting protein of *Amphidinium*—characterization and relation to other light-harvesting proteins, *Photochem. Photobiol.* **57**, 125–131.
 31. Iglesias-Prieto, R., Govind, N. S., and Trench, R. K. (1993) Isolation and characterization of 3 membrane-bound chlorophyll-protein complexes from 4 dinoflagellate species, *Philos. Trans. R. Soc. London, Ser. B* **340**, 381–392.
 32. Jovine, R. V. M., Johnsen, G., and Prezelin, B. B. (1995) Isolation of membrane-bound light-harvesting complexes from the dinoflagellates *Heterocapsa pygmaea* and *Prorocentrum minimum*, *Photosynth. Res.* **44**, 127–138.
 33. Hiller, R. G., Wrench, P. M., and Sharples, F. P. (1995) The light-harvesting chlorophyll a/c binding protein of dinoflagellates—a putative polyprotein, *FEBS Lett.* **363**, 175–178.
 34. Büchel, C. (2003) Fucoxanthin-chlorophyll proteins in diatoms: 18 and 19 kDa subunits assemble into different oligomeric states, *Biochemistry* **42**, 13027–13034.
 35. Sharples, F. P., Wrench, P. M., Ou, K. L., and Hiller, R. G. (1996) Two distinct forms of the peridinin-chlorophyll alpha-protein from *Amphidinium carterae*, *Biochim. Biophys. Acta* **1276**, 117–123.
 36. van Stokkum, I. H. M., Larsen, D. S., and van Grondelle, R. (2004) Global and target analysis of time-resolved spectra, *Biochim. Biophys. Acta* **1657**, 82–104.
 37. Polívka, T., Zigmantas, D., Sundström, V., Formaggio, E., Cinque, G., and Bassi, R. (2002) Carotenoid S_1 state in a recombinant light-harvesting complex of photosystem II, *Biochemistry* **41**, 439–450.
 38. Zhang, J.-P., Fujii, R., Qian, P., Inaba, T., Mizoguchi, T., Koyama, Y., Onaka, K., Watanabe, Y., and Nagae, H. (2000) Mechanism of the carotenoid-to-bacteriochlorophyll energy transfer via the S_1 state in the LH2 complexes from purple bacteria, *J. Phys. Chem. B* **104**, 3683–3691.
 39. Polívka, T., Pullerits, T., Frank, H. A., Cogdell, R. J., and Sundström, V. (2004) Ultrafast formation of a carotenoid radical in LH2 antenna complexes of purple bacteria, *J. Phys. Chem. B* **108**, 15398–15407.
 40. Liu, Z. F., Yan, H. C., Wang, K. B., Kuang, T. Y., Zhang, J. P., Gui, L. L., An, X. M., and Chang, W.R. (2004) Crystal structure of spinach major light-harvesting complex at 2.72 Å resolution, *Nature* **428**, 287–292.
 41. Novoderezhkin, V. I., Palacios, M. A., van Amerongen, H. and van Grondelle R. (2005) Excitation dynamics in the LHCI complex of higher plants: Modeling based on the 2.72 Å crystal structure, *J. Phys. Chem. B* **109**, 10493–10504.
 42. Billsten, H. H., Zigmantas, D., Sundström, V. and Polívka, T. (2002) Dynamics of vibrational relaxation in the S_1 state of carotenoids having 11 conjugated C=C bonds, *Chem. Phys. Lett.* **355**, 465–470.
 43. de Weerd, F. L., van Stokkum, I. H. M., and van Grondelle, R. (2002) Subpicosecond dynamics in the excited-state absorption of all-trans β -carotene, *Chem. Phys. Lett.* **354**, 38–43.
 44. Frank, H. A., Cua, A., Chynwat, V., Young, A., Gosztola, D., and Wasielewski, M. R. (1996) The lifetimes and energies of the first excited singlet states of diadinoxanthin and diatoxanthin: The role of these molecules in excess energy dissipation in algae, *Biochim. Biophys. Acta* **1277**, 243–252.
 45. Ilagan, R. P., Christensen, R. L., Chapp, T. W., Gibson, G. N., Pascher, T., Polivka, T., and Frank, H. A. (2005) Femtosecond time-resolved absorption spectroscopy of astaxanthin in solution and in alpha-crustacyanin, *J. Phys. Chem. A* **109**, 3120–3127.
 46. Gradinaru, C. C., Kennis, J. T. M., Papagiannakis, E., van Stokkum, I. H. M., Cogdell, R. J., Fleming, G. R., Niederman, R. A., and van Grondelle, R. (2001) An unusual pathway of excitation energy deactivation in carotenoids: Singlet-to-triplet conversion on an ultrafast timescale in a photosynthetic antenna, *Proc. Natl. Acad. Sci. U.S.A.* **98**, 2364–2369.
 47. Larsen, D. S., Papagiannakis, E., van Stokkum, I. H. M., Vengris, M., Kennis, J. T. M., and van Grondelle, R. (2003) Excited-state dynamics of beta-carotene explored with dispersed multi-pulse transient absorption, *Chem. Phys. Lett.* **381**, 733–742.
 48. Johnsen, G., Prezelin, B. B., and Jovine, R. V. M. (1997) Fluorescence excitation spectra and light utilization in two red tide dinoflagellates, *Limnol. Oceanogr.* **42**, 1166–1177.

49. Latasa, M. (1995) Pigment composition of *Heterocapsa* sp. and *Thalassiosira weissflogii* growing in batch cultures under different irradiances, *Sci. Mar.* 59, 25–37.
50. Holt, N.E., Zigmantas, D., Valkunas, L., Li, X. P., Niyogi, K. K., and Fleming, G. R. (2005) Carotenoid cation formation and the regulation of photosynthetic light harvesting, *Science* 307, 433–436.
51. Pascal, A. A., Liu, Z. F., Broess, K., van Oort, B., van Amerongen, H., Wang, C., Horton, P., Robert, B., Chang, W. R., and Ruban, A. (2005) Molecular basis of photoprotection and control of photosynthetic light-harvesting, *Nature* 436, 134–137.
52. Ilagan, R. P., Shima, S., Melkozernov, A., Lin, S., Blankenship, R. E., Sharples, F. P., Hiller, R. G., Birge, R. R., and Frank, H. A. (2004) Spectroscopic properties of the main-form and high-salt peridinin-chlorophyll a proteins from *Amphidinium carterae*, *Biochemistry* 43, 1478–1487.

BI060265B